RSC Advances

PAPER

View Article Online
View Journal | View Issue

Cite this: *RSC Adv.*, 2025, **15**, 38211

Role of surface oxygen functional groups in the adsorption of catechol, hydroquinone, and aniline on graphene oxide

Md Samiur Rahman, Anggon Barua, Sharifa Faraezi * and Md Sharif Khan *

Catechol (CT), hydroquinone (HQ), and aniline (AN) are environmentally significant aromatic pollutants that pose severe risks to human health even at trace levels. Their structural similarity makes selective detection and removal challenging, particularly on carbon-based adsorbents such as graphene oxide (GO). In this work, all-atom molecular dynamics (MD) simulations were employed to investigate the interfacial structure, dynamics, and adsorption behavior of CT, HQ, and AN on GO surfaces functionalized with epoxide (–O–), hydroxyl (–OH), and carboxyl (–COOH) groups. CT and HQ, as positional isomers, were compared to assess the impact of hydroxyl group arrangement, while AN served to evaluate the influence of a different functional group ($–NH_2$). Radial distribution function analysis revealed strong hydrogen-bonding interactions between molecular functional groups and oxygen-containing surface functionalities, with distinct second-neighbor peaks for CT and AN linked to their molecular geometry. HQ exhibited island-like aggregation on the surface, enabling simultaneous interaction *via* both hydroxyl groups and the aromatic ring, leading to enhanced affinity for –O– sites but reduced accessibility to –COOH groups. Native contact analysis indicated a parallel adsorption geometry for HQ, while CT and AN preferentially interacted *via* hydroxyl or amine-linked hydrogens. Interaction energy calculations confirmed that HQ had the strongest –O– affinity, whereas CT and AN showed balanced but slightly higher interactions with –O– and –COOH compared to –OH. These results elucidate the role of both surface chemistry and molecular structure in determining adsorption preferences and mobility, providing molecular-level guidelines for designing GO-based sensing and separation platforms for aromatic contaminants.

Received 16th August 2025
Accepted 9th October 2025

DOI: 10.1039/d5ra06051f

rsc.li/rsc-advances

1. Introduction

Catechol (CT) and hydroquinone (HQ) are frequently coexisting isomers of phenolic compounds in nature, widely used in cosmetics, dyes, pesticides, and pharmaceutical industries.[1–3] Owing to their toxicological impact, numerous environmental protection agencies have identified CT and HQ as primary contaminants and have established maximum permissible concentration in drinking water.[4–7] Likewise, Aniline (AN) is also used in different industries as a raw material.[8–10] which can undergo diverse chemical processes, including oxidation, diazotization, and acylation, and its use poses significant risks to both human health and the environment.[11–14] Even at low concentrations, these compounds are toxic to various species and can adversely affect human health, they are classified as priority and hazardous pollutants.[15–17] Despite their environmental relevance, selective detection of these benzene derivatives remains challenging due to their closely related aromatic structures, which differ only in functional group composition and the location of the functional groups in the structure.[18,19] Given their pronounced sensitivity to carbon-based materials,[15,20] these findings pave the way for the rational design of modified carbon surfaces with tailored functional groups, enabling the selective identification of CT, HQ, and AN through their distinctive –OH and–NH_2 interaction patterns.

Traditional approaches for the detection and removal of CT, HQ, and AN include electrochemical sensors,[21] adsorption,[22] column gas chromatography,[23] incineration,[23] catalytic oxidation[24] from aqueous solutions. Among these, adsorption has an advantage over other technologies in terms of cost due to its simplicity.[25–27] The efficiency of adsorption depends strongly on the surface properties of the adsorbent, including its chemical and mechanical stability, broad specific surface area, accessibility, and affinity toward target molecules.[28,29]

Functionalized graphene and fabricated graphene have been used for diverse technological applications including sensing or capturing flow gasses,[30,31] energy storage systems,[32,33] simultaneous detection of hazardous chemicals[34] *etc.* One of the common functionalized form of graphene, graphene oxide (GO) possess high specific surface area and oxygen containing functional groups is widely used to remove hazardous

Center for Interdisciplinary Chemistry Research-CICR, Bangladesh. E-mail: faraezinp@gmail.com; sharifkhanjnu@gmail.com

compounds through the adsorption technique.[22,35] Numerous theoretical and experimental studies have been conducted to evaluate the interaction, chemical stability, sensitivity, and diffusivity of phenolic derivatives on graphene oxide.[36–41] For instance, Tran *et al.* measured the redox potential of aromatic compounds with varying hydroxyl groups on graphene oxide using cyclic voltammetry. They found *ortho-* and *para-*substituted phenols show the greatest electrochemical sensitivity to graphene oxide surface.[42] Yi *et al.* showed that the ACS/GO composite (GO well-dispersed, 7.46 m^2 g^{-1}) efficiently adsorbs aniline from water (Freundlich and Langmuir models, pseudo-second-order kinetics) and enhances adsorption from cigarette smoke.[43] Xiaobo Li *et al.* investigated HQ and CT sensitivity at a thionine/graphene oxide modified glassy carbon electrode electrochemically and showed that the TH-GO/GCE sensor enables sensitive, reproducible detection of HQ and CT with low detection limits, wide linear range, and applicability to real samples and other analytes.[44]

In recent years, Molecular Dynamics (MD) simulations have emerged as a powerful tool to gain detailed insights into the interfacial mechanism, dynamics, and adsorption behaviours in large and complex systems.[45–47] Tang *et al.* studied the adsorption capacity of aromatic compounds on GO using MD simulations and Density Function Theory (DFT) calculations.[48] The charge transfer mechanism of CT molecules on ZnO and RGO/ZnO clusters was examined experimentally, and further validated through DFT calculations.[49] Li *et al.* showed *via* MD simulations that phenol adsorption into GO interlayers is spontaneous, π–π and hydrogen-bonding driven, and controlled by interlayer spacing and oxidation.[50]

Despite extensive research, the molecular-level understanding of the interfacial structure and dynamics of HQ, CT, and AN on graphene oxide (GO) remains limited—particularly regarding the influence of GO's surface functional groups on adsorption behavior, as well as the local molecular interactions with the surface. In this work, we employed all-atom molecular dynamics (MD) simulations to investigate the interfacial structure and dynamics of CT, HQ, and AN on GO. The structural differences between CT and HQ, arising from the distinct positions of their hydroxyl groups, were examined to elucidate positional effects, while AN was used to assess the influence of a different functional group (–NH_2) on adsorption. Various oxygen-containing surface functionalities of GO, including epoxide (–O–), hydroxyl (–OH), and carboxyl (–COOH) groups, were considered to identify the most favourable functional group for selective sensing.

2. Computational method

All atom MD simulations were performed using GROMACS simulation package. The simulation setup comprise a single-layer graphene oxide (GO) sheet of dimensions 5 × 5 nm and 100 organic molecules. The GO sheet was modelled following the Lerf–Klinowski[51] structural model using the GOPY tool,[52] as python-base package developed for generating functionalized graphene surfaces. In this model, carboxylic groups were attached to the edge of the GO sheet, whereas hydroxyl and epoxy groups were attached onto the basal plane. The overall chemical composition of the GO structure was $C_{30}(–O–)_1(OH)_1(COOH)_{0.5}$ consistent with the structure reported elsewhere.[48,53] This choice provides a reproducible and tractable representation that includes the principal oxygen-containing functionalities. We emphasize that this model is an idealized, average description, while experimentally prepared GO samples commonly exhibit a wider range of functional group densities and heterogeneous spatial distributions that depend on the synthetic route and post-treatment. Three types of fully atomistic organic molecules, such as CT, HQ, and AN were used tin the simulations. The AMBER force field was employed for both the GO surface and the organic molecules. The AMBER force field has previously been validated for adsorption processes on graphene and graphene oxide surfaces, including systems exhibiting π–π stacking and hydrogen bonding, such as DNA adsorption on GO and reduced GO-PEG-NH_2 in electrolyte solutions.[54–56] Non bonded interactions were described using the standard 12–6 Lennard-Jones (LJ) potential, and electrostatic interactions were calculated using the particle–particle particle-mesh method with a cut off distance of 1.2 nm.[57,58] Lorentz–Berthelot mixing rules were applied to determine the LJ parameters for unlike atom pairs across different components. For each system, 100 organic molecules were randomly distributed near to the GO surface within a three-dimensional periodic simulation box. A vacuum space of 120 nm was introduced along the *z*-axis to prevent the long range interactions between the periodic images. All simulations were conducted in the NVT ensemble at 298 K using the Nosé–Hoover thermostat. Each system was equilibrated for 5 ns with a timestep of 0.001 ps. Convergence was verified by monitoring both the total potential energy (Fig. S1) and the center-of-mass distances between the adsorbates and the GO surface (Fig. S2), which stabilized within the few nanoseconds, confirming that a 5 ns trajectory was sufficient to reach the equilibrium.

3. Results and discussion

3.1 Atomic and surface structure

Fig. 1(a) presents the ball and stick representation of the GO surface and the CT, HQ, and AN molecules. The GO surface

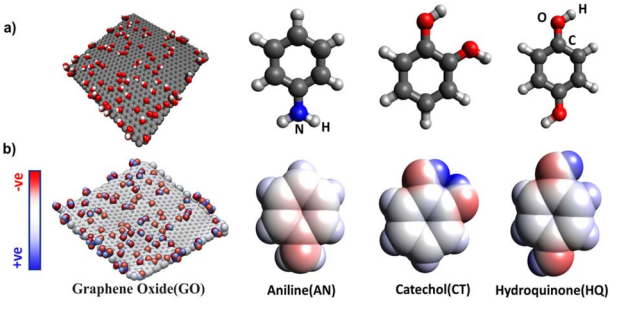

Fig. 1 (a) van-der-Waals structure of graphene oxide (GO), where hydrogen (white), carbon (grey), and oxygen (red) and ball-stick structure of the AN, CT and HQ, where hydrogen (white), carbon (grey), nitrogen (blue) and oxygen (red). (b) partial charge distribution per atom in GO, AN, CT, and HQ.

incorporates three distinct functional groups, including epoxy (–O–), hydroxyl (–OH–), and carboxyl (–COOH). CT and HQ are structural isomers, each containing two hydroxyl groups attached to a benzene ring but differing in their relative positions. In contrast, AN features an amine group bonded to the benzene ring. The presence of these functional groups on the GO surface results in a heterogeneous charge distribution, a characteristic that also applies to the CT, HQ, and AN molecules. To quantify this effect, partial atomic charges were computed using the AM1-BCC method. As illustrated in Fig. 1(b), charge polarization, both positive and negative is localized primarily around the functional groups of the GO surface and the organic molecules.

3.2 Interfacial structure

Fig. 2 (a–c) depicts the temporal evolution of the distance and population of HQ, CT, and AN molecules relative to the GO surface. The distance was calculated as the separation between the surface and the center of mass of each molecule. Over the course of the simulations, all three types of molecules progressively approached the surface. However, HQ consistently remained at a slightly greater distance from the surface compared to CT and AN, even after equilibration. The average distances, shown in Fig. S2, indicate that HQ remained approximately 6.2 Å from the surface, whereas CT and AN were positioned at around 4.7 Å.

The lower panel of Fig. 2 presents the spatial distribution of HQ, CT, and AN distances from the surface, derived from the final simulation snapshot. In this representation, violet color corresponds to the shortest distances and transitions to yellow as the distance increases. HQ exhibits distinct yellow regions, indicating that a fraction of HQ molecules reside at around 9 Å from the surface, which is not the case for CT and AN. This observation suggests that HQ molecules tend to aggregate into surface bound islands through strong intermolecular interactions, whereas CT and AN molecules are more uniformly distributed across the surface with comparatively weaker intermolecular interactions. The origin of the intermolecular interactions in HQ is governed by the *para* position of its –OH groups, as confirmed by the RDFs between HQ molecules (Fig. S3), which display a pronounced peak at ~0.6 nm, which is missing for the other two molecules, indicating a strong correlations between –OH groups of the neighboring HQ molecules. Additional initial and final snapshots of the simulation systems were depicted in Fig. S4.

The simulated radial distribution functions (RDFs) describing the correlations between HQ, CT, and AN molecules and the oxygen atoms of surface functional groups (–COOH, –OH, and –O–) are presented in Fig. 3(a–c). For HQ and CT, the correlations were calculated between the oxygen and hydrogen atoms of their functional groups and the oxygen atoms of the surface functional groups, whereas for AN, the nitrogen and hydrogen atoms were considered. For –COOH groups, strong correlations were observed between the oxygen atoms of –COOH and the oxygen and hydrogen atoms of CT, as well as the nitrogen and hydrogen atoms of AN, relative to HQ. The first-neighbor distances between the oxygen atoms of –COOH and the oxygen atoms of HQ, CT, and the nitrogen atoms of AN were 0.31 nm, 0.30 nm, and 0.30 nm, respectively. Corresponding distances for the hydrogen atoms of HQ, CT, and AN were shorter, at 0.20 nm, 0.20 nm, and 0.22 nm, respectively. For –OH groups on the surface, the first-neighbor distances between the oxygen atoms of HQ, CT, and the nitrogen atoms of AN and the oxygen atoms of the –OH groups were 0.30 nm, 0.30 nm, and 0.31 nm, respectively. For hydrogen atoms, the distances were 0.21 nm, 0.21 nm, and 0.22 nm, respectively. For –O– groups, the first-neighbor distances between the oxygen atoms of HQ, CT, and the nitrogen atoms of AN and the oxygen atoms of –O– groups were 0.28 nm, 0.30 nm, and 0.30 nm, respectively, whereas the hydrogen atoms of HQ, CT, and AN coordinated at distances of 0.18 nm, 0.20 nm, and 0.20 nm, respectively. In addition, hydrogen correlations for CT and AN exhibited a distinct second-neighbor peak, attributable to the presence of adjacent functional groups, two hydroxyls in *ortho* positions for CT and two hydrogens in the $–NH_2$ group of AN. This peak was absent for HQ due to the *para*-positioned hydroxyl groups,

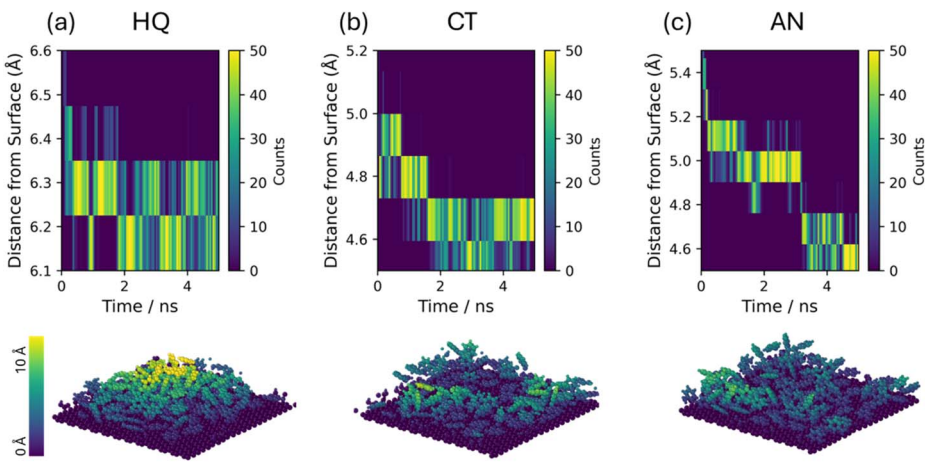

Fig. 2 Changes of the distances from surface and the amount of HQ (a), CT (b), and AN (c) as a function of temperature. Corresponding simulation snapshots with the final distances of the HQ, CT and AN from the surface (bottom panel).

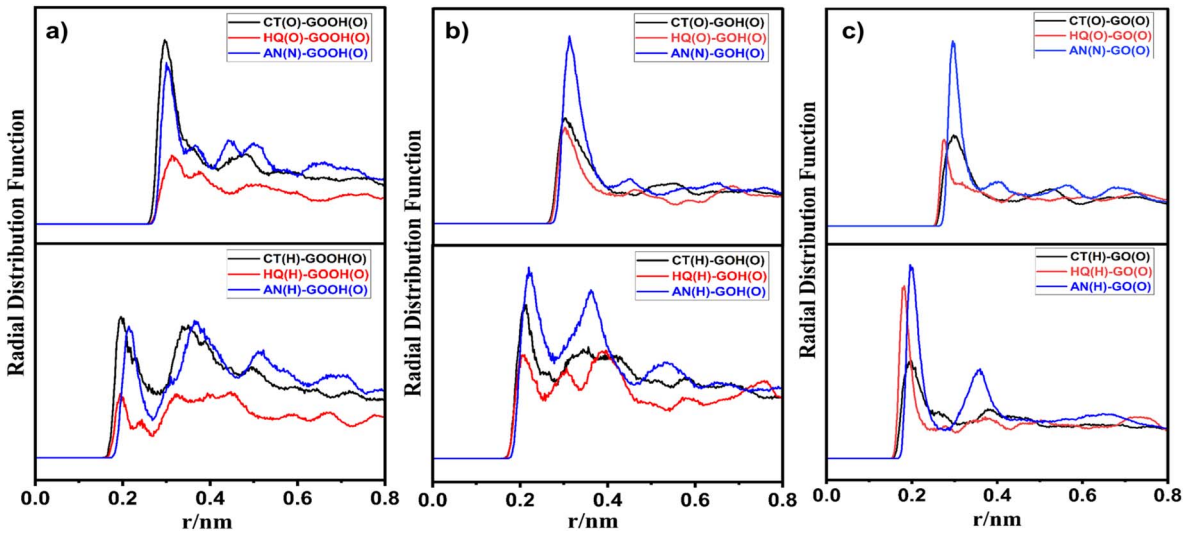

Fig. 3 Simulated radial distribution function (RDF) of CT (black), HQ (red), and AN (blue) with different surface functional groups (a) –COOH, (b) –OH, (c) –O–. Top panels show O/N and bottom panels show H correlation with the surface functional groups.

which are too far apart to simultaneously correlate with the same surface functional group. Overall, the short first-neighbor distances between the hydrogen atoms of HQ, CT, and AN functional groups and the oxygen atoms of the surface functional groups are consistent with O–H hydrogen bonding,[59] while slightly longer distances were observed for $–NH_2$ groups, as expected. Despite similar O–H correlations for –COOH and –OH surface groups, –O– groups exhibited slightly shorter distances, a trend most pronounced for HQ, likely due to the positional arrangement of its functional groups.

The structural arrangement of the molecules on the GO surface significantly influences their interactions with surface functional groups. Simulated snapshots, shown in Fig. 4, reveal that the hydrogen atoms of the functional groups of organic molecules predominantly interact with the oxygen atoms of various surface functional groups. HQ is capable of simultaneously interacting with two surface functional groups *via* its two hydroxyl groups. In contrast, CT primarily engages with only one surface functional group, despite possessing two hydroxyl groups; the second hydroxyl forms an intramolecular hydrogen bond due to its structural position. Similarly, AN interacts with only one surface functional group, while its other hydrogen remains far from the adsorption site, a behaviour consistent with the presence of a distinct second-neighbor peak in the RDFs.

We further quantified the native contacts between the hydroxyl groups (OH–GO) and aromatic rings (ring–GO) of the organic molecules and the GO surface by calculating the number of contacts over the course of the simulations (Fig. 5). HQ exhibited an equal number of native contacts with the GO surface through both its hydroxyl groups and aromatic ring, indicating that HQ interacts with the surface *via* both functional groups simultaneously. This interaction pattern is consistent with a parallel orientation of HQ relative to the GO surface, a behavior also reported in previous studies.[60]

In contrast, CT and AN showed a higher number of OH–GO contacts compared to ring–GO contacts, indicating that their interactions with the GO surface are predominantly mediated through the hydroxyl (for CT) or amine-linked hydrogen (for AN) groups rather than direct π–π stacking of the aromatic ring. Among the three molecules, CT exhibited the highest number of OH–GO contacts, in agreement with earlier reports involving polymer-modified glassy carbon electrodes and pristine graphene.[60,61] The comparatively lower number of native contacts for HQ relative to CT and AN can be attributed to the island-like aggregation of HQ molecules observed in Fig. 2, which limits the accessible surface area for direct contact. Additionally, the simultaneous engagement hydroxyl groups of HQ and aromatic ring likely requires a greater spatial footprint, further reducing the overall number of contacts per molecule.

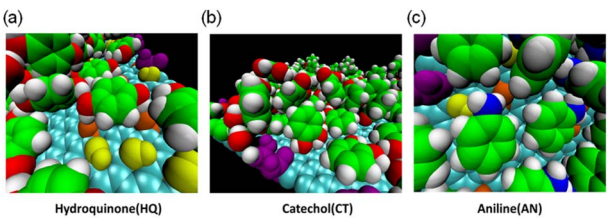

Fig. 4 Simulated snapshot on GO functional groups interacting with (a) HQ, (b) CT, and (c) AN, where graphene (cyan), epoxy group (orange), hydroxyl group (yellow), carboxylic group (purple), oxygen (red), blue (nitrogen), and hydrogen (white).

3.3 Interaction energy and dynamics

The interaction energies presented in Fig. 6 provide insight into the specific affinities between the surface functional groups of GO and the functional groups of the organic molecules. This interaction energies between the GO functional groups and the organic molecules were calculated and normalized by dividing by the number of organic molecules in the system. Error

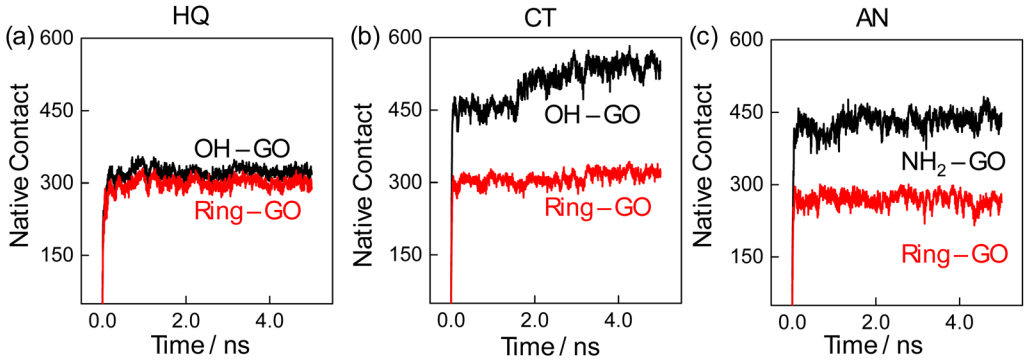

Fig. 5 Simulated amount of native contact between the GO surface and OH (black), and benzene ring (red) of the HQ (a), CT (b), and AN (c) as a function of the simulation time.

estimates were obtained by block averaging of the trajectories, and the corresponding standard deviations are shown as error bars in Fig. 6. For the –O– and –OH surface functional groups, the interaction energies with the functional groups of organic molecules are comparable. However, for the –COOH group, HQ exhibits a significantly higher energy compared to CT and AN. Presumably, –COOH groups are likely less accessible to HQ due to its adsorption geometry, engaging both hydroxyl groups and the aromatic ring in parallel contact with the surface and its tendency to form densely packed islands *via* strong intermolecular interactions. Such aggregation can limit the ability of HQ molecules to reorient and access all surface sites. Furthermore, the interactions with surface –COOH groups are primarily mediated by the functional moieties of the organic molecules. As shown in Fig. S6, the overall interaction energy contribution of the molecules is less for –COOH groups than for the other surface functional groups.

HQ can adopt configurations that strongly favor interaction with –O– groups by positioning itself between two adjacent –O– sites, thereby enabling both hydroxyl groups to form simultaneous hydrogen bonds, as suggested by the simulated snapshots in Fig. 4. This dual-site binding likely contributes to the stability of HQ's surface association and explains its pronounced –O– interaction energy. The combination of strong –O– interactions and island formation also results in reduced lateral mobility for HQ, as evidenced by the lower displacement values shown in Fig. S5, relative to CT and AN.

In contrast, CT and AN display more evenly distributed interaction energies across all three surface functional groups, with a slight preference for –O– and –COOH groups over –OH groups. AN exhibits marginally higher displacement than CT, which may be attributed to the presence of one unbound hydrogen in its $-NH_2$ group, providing additional conformational flexibility. Whereas, CT is capable of forming an intramolecular hydrogen bond between its two hydroxyl groups, which can reduce molecular flexibility and mobility on the surface.

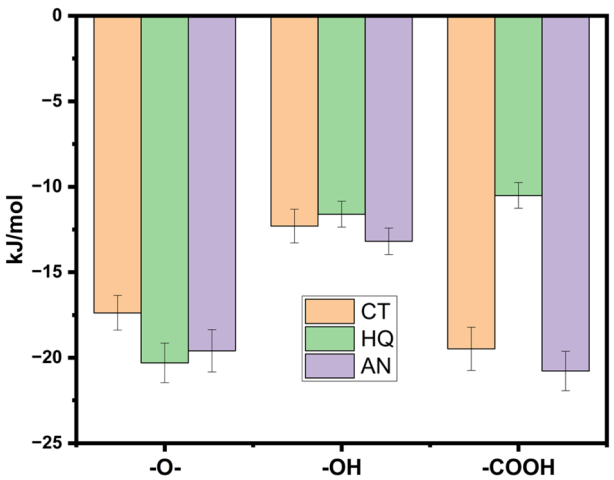

Fig. 6 Interaction energies between surface functional groups and functional groups of CT, HQ, and AN.

4. Conclusions

This study provides a detailed molecular-level understanding of the adsorption mechanisms of CT, HQ, and AN on graphene oxide functionalized with –O–, –OH, and –COOH groups. The simulations demonstrate that the positional arrangement of hydroxyl groups in CT and HQ, as well as the presence of an amine group in AN, critically influence adsorption geometry, surface affinity, and mobility. HQ exhibits a unique dual-site adsorption mode, interacting simultaneously through hydroxyl groups and the aromatic ring, which promotes aggregation into surface-bound islands and preferential binding to –O– sites. This configuration limits accessibility to –COOH groups and reduces lateral displacement. In contrast, CT and AN favour –O– and –COOH functionalities, with CT exhibiting the highest number of OH–GO contacts and AN showing greater mobility due to its unbound amine hydrogen. The combination of RDF analysis, native contact quantification, and interaction energy evaluation underscores the interplay between molecular geometry and surface chemistry in driving selective adsorption. Although the present simulations do not aim to reproduce experimental adsorption isotherms, available batch-adsorption studies on GO and GO-based composites report that CT, HQ and AN are readily adsorbed *via* combined π–π stacking and hydrogen-bonding mechanism.[62,63] These experimental

observations are consistent with our atomistic results, which identify hydrogen bonding with oxygenated surface sites and aromatic-ring interactions as the dominant binding motifs. From an experimental standpoint, enrichment of –COOH groups at sheet edges is expected to enhance CT and AN adsorption, whereas increasing basal-plane epoxide density would favour HQ adsorption while also contributing to CT and AN binding. These findings offer a framework for engineering GO-based materials with tailored functionalization to enhance the selective sensing, separation, and removal of structurally similar aromatic pollutants from aqueous environments.

Author contributions

Md Samiur Rahman: writing – original draft, methodology, data curation, investigation, formal analysis. Anggon Barua: methodology, formal analysis, investigation. Sharifa Faraezi: conceptualization, supervision, validation, writing – review and editing, funding acquisition. Md Sharif Khan: writing – review and editing, supervision, funding acquisition.

Conflicts of interest

There are no conflicts to declare.

Data availability

The data that support the findings of this study are included in this article are available from the corresponding authors upon reasonable request.

Supplementary information: changes of total potential energy over simulation time, change of the distance between GO and adsorbed molecules, intermolecular RDFs of CT, HQ and AN, initial and final simulated snapshots, mean square displacement of organic molecules, total interaction energy between the GO and organic molecules. See DOI: **https://doi.org/10.1039/d5ra06051f**.

Acknowledgements

This research is funded by the Center for Interdisciplinary Chemistry Research (CICR), Bangladesh.

Notes and references

1 H. Du, J. Ye, J. Zhang, X. Huang and C. Yu, *J. Electroanal. Chem.*, 2011, **650**, 209–213.
2 Z. Y. Lin, Y. C. Kuo, C. J. Chang, Y. S. Lin, T. C. Chiu and C. C. Hu, *RSC Adv.*, 2018, **8**, 19381–19388.
3 M. Aragó, C. Ariño, À. Dago, J. M. Díaz-Cruz and M. Esteban, *Talanta*, 2016, **160**, 138–143.
4 Y. Wang, Y. Xiong, J. Qu, J. Qu and S. Li, *Sensor. Actuator. B Chem.*, 2016, **223**, 501–508.
5 K. Harikrishnan, G. Singh, A. Kushwaha, V. P. Singh, U. K. Gaur and M. Sharma, *J. Environ. Chem. Eng.*, 2022, **10**, 108717.
6 Z. C. Fan, Z. Li, X. Y. Wei, Q. Q. Kong, Z. Q. Liu, L. Li, J. H. Li, F. Yin, K. L. Lu and Z. M. Zong, *Microchem. J.*, 2022, **182**, 107880.
7 Y. Zhang, Y. Li and S. Tabassum, *J. Water Process Eng.*, 2024, **61**, 105286.
8 V. Alagarsamy, V. Raja Solomon and K. Dhanabal, *Bioorganic Med. Chem.*, 2007, **15**, 235–241.
9 Z. Fan, S. Zheng, H. Zhang, K. Chen, Y. Li, C. Liu, S. Xiang and Z. Zhang, *Chinese Chem. Lett.*, 2022, **33**, 4317–4320.
10 A. Grirrane, A. Corma and H. García, *Science*, 2008, **322**, 1661–1664.
11 W. Li, J. Zhang, L. Fan, Y. Zhao, C. Sun, W. Li and Z. Chang, *Spectrochim. Acta, Part A*, 2024, **314**, 124223.
12 N. K. Chaturvedi, *Appl. Water Sci.*, 2022, **12**, 1–15.
13 M. Mohammed, L. P. Mekala, S. Chintalapati and V. R. Chintalapati, *J. Hazard. Mater.*, 2020, **385**, 121571.
14 S. Ghosh, A. Malloum, C. Bornman, A. Othmani, C. Osagie, Z. K. Esfahani, W. A. Khanday, S. Ahmadi and M. H. Dehghani, *J. Mol. Liq.*, 2022, **345**, 118167.
15 W. Zhang, W. Wang, S. Liu, N. Tian, Q. Sun and Z. Wu, *Appl. Surf. Sci.*, 2024, **649**, 159114.
16 H. Yin, Q. Zhang, Y. Zhou, Q. Ma, T. Liu, L. Zhu and S. Ai, *Electrochim. Acta*, 2011, **56**, 2748–2753.
17 M. K. Abugazleh, H. M. Ali, J. A. Chester, A. M. Al-Fa'ouri and J. L. Bouldin, *Ecotoxicology*, 2023, **32**, 656–665.
18 M. Zhang, C. Y. Ge, Y. F. Jin, L. Bin Hu, H. Z. Mo, X. B. Li and H. Zhang, *J. Chem.*, 2019, **2019**, 2327064.
19 M. U. Hossain, M. T. Rahman and M. Q. Ehsan, *Int. J. Anal. Chem.*, 2015, **2015**, 862979.
20 X. Cheng, X. Shui, Q. Yang, H. Ma, Y. Zhang, T. Zeng, J. Yang, Z. Wu, X. Zhang and N. Yang, *Anal. Chim. Acta*, 2025, **1357**, 344074.
21 B. Unnikrishnan, P. L. Ru and S. M. Chen, *Sensor. Actuator. B Chem.*, 2012, **169**, 235–242.
22 A. Abu-Nada, A. Abdala and G. McKay, *J. Environ. Chem. Eng.*, 2021, **9**, 105858.
23 E. J. Nanni, M. E. Lovette, R. D. Hicks, K. W. Fowler and M. F. Borgerding, *J. Chromatogr. A*, 1990, **505**, 365–374.
24 S. Zhang, X. Zhao, H. Niu, Y. Shi, Y. Cai and G. Jiang, *J. Hazard. Mater.*, 2009, **167**, 560–566.
25 R. Rashid, I. Shafiq, P. Akhter, M. J. Iqbal and M. Hussain, *Environ. Sci. Pollut. Res.*, 2021, **288**, 9050–9066.
26 B. S. Rathi and P. S. Kumar, *Environ. Pollut.*, 2021, **280**, 116995.
27 M. N. Rashed and M. N. Rashed, *Org. Pollut. – Monit. Risk Treat.*, 2013, DOI: **10.5772/54048**.
28 M. M. Aljohani, S. D. Al-Qahtani, M. Alshareef, M. G. El-Desouky, A. A. El-Bindary, N. M. El-Metwaly and M. A. El-Bindary, *Process Saf. Environ. Prot.*, 2023, **172**, 395–407.
29 T. E. Akinola, P. L. Bonilla Prado and M. Wang, *Appl. Energy*, 2022, **317**, 119156.
30 R. Stuart Haszeldine, *Science*, 2009, **325**, 1647–1652.
31 S. M. Khan, H. Kitayama, Y. Yamada, S. Gohda, H. Ono, D. Umeda, K. Abe, K. Hata and T. Ohba, *J. Phys. Chem. C*, 2018, **122**, 24143–24149.
32 S. Faraezi, M. S. Khan and T. Ohba, *Ind. Eng. Chem. Res.*, 2020, **59**, 5768–5774.

33 J. Azadmanjiri, V. K. Srivastava, P. Kumar, M. Nikzad, J. Wang and A. Yu, *J. Mater. Chem. A*, 2018, **6**, 702–734.
34 L. Wang, Y. Zhang, Y. Du, D. Lu, Y. Zhang and C. Wang, *J. Solid State Electrochem.*, 2012, **16**, 1323–1331.
35 R. Zhao, Y. Li, J. Ji, Q. Wang, G. Li, T. Wu and B. Zhang, *Colloids Surf., A*, 2021, **611**, 125866.
36 Y. Wang, F. Zhai, Y. Hasebe, H. Jia and Z. Zhang, *Bioelectrochemistry*, 2018, **122**, 174–182.
37 P. Stathi, D. Gournis, Y. Deligiannakis and P. Rudolf, *Langmuir*, 2015, **31**, 10508–10516.
38 A. Molla, Y. Li, B. Mandal, S. G. Kang, S. H. Hur and J. S. Chung, *Appl. Surf. Sci.*, 2019, **464**, 170–177.
39 S. Muthusaravanan, K. Balasubramani, R. Suresh, R. S. Ganesh, N. Sivarajasekar, H. Arul, K. Rambabu, G. Bharath, V. E. Sathishkumar, A. P. Murthy and F. Banat, *Environ. Res.*, 2021, **200**, 111428.
40 P. Pal, A. Yadav, P. S. Chauhan, P. K. Parida and A. Gupta, *Sensors Int.*, 2021, **2**, 100072.
41 X. Wang, Y. Hu, J. Min, S. Li, X. Deng, S. Yuan and X. Zuo, *Appl. Sci.*, 2018, **8**(8), 1950.
42 T. M. H. Tran, A. Ambrosi and M. Pumera, *Phys. Chem. Chem. Phys.*, 2016, **18**, 30515–30519.
43 Z. Yi, L. Huajie, L. Mingchun and X. Meihua, *J. Mol. Struct.*, 2020, **1209**, 127973.
44 X. Li, G. Xu, X. Jiang and J. Tao, *J. Electrochem. Soc.*, 2014, **161**, 464–468.
45 R. Wang, M. L. Klein, V. Carnevale and E. Borguet, *Wiley Interdiscip. Rev. Comput. Mol. Sci.*, 2021, **11**, e1537.
46 Z. Taheri and A. Nakhaei Pour, *J. Mol. Model.*, 2021, **27**, 1–8.
47 M. Huang, H. Zhang, Y. Gao and L. Wang, *Int. J. Pavement Eng.*, 2021, **22**, 319–330.
48 H. Tang, Y. Zhao, S. Shan, X. Yang, D. Liu, F. Cui and B. Xing, *Environ. Sci. Technol.*, 2018, **52**, 7689–7697.
49 R. Ponnusamy, R. Venkatesan, A. Gangan, R. Samal, B. Chakraborty, D. J. Late and C. S. Rout, *Appl. Surf. Sci.*, 2019, **495**, 143588.
50 J. Li, Q. Li, Z. Xu and X. Yang, *Sep. Purif. Technol.*, 2024, **335**, 126215.
51 A. Lerf, H. He, M. Forster and J. Klinowski, *J. Phys. Chem. B*, 1998, **102**, 4477–4482.
52 S. Muraru, J. S. Burns and M. Ionita, *SoftwareX*, 2020, **12**, 100586.
53 H. Tang, D. Liu, Y. Zhao, X. Yang, J. Lu and F. Cui, *J. Phys. Chem. C*, 2015, **119**, 26712–26718.
54 S. Muraru, C. G. Samoila, E. I. Slusanschi, J. S. Burns and M. Ionita, *Coatings*, 2020, **10**, 289.
55 J. Chen, L. Chen, Y. Wang and S. Chen, *J. Phys. D Appl. Phys.*, 2014, **47**, 505401.
56 Z. Xu, X. Lei, Y. Tu, Z. J. Tan, B. Song and H. Fang, *Chem.–Eur. J*, 2017, **23**, 13100–13104.
57 Y. Li, M. Liao and J. Zhou, *J. Phys. Chem. C*, 2018, **122**, 22965–22974.
58 J. Comer, R. Chen, H. Poblete, A. Vergara-Jaque and J. E. Riviere, *ACS Nano*, 2015, **9**(12), 11761–11774.
59 Y. Wu, X. Zhang, C. Liu, L. Tian, Y. Zhang, M. Zhu, W. Qiao, J. Wu, S. Yan, H. Zhang and H. Bai, *ACS Omega*, 2024, **9**, 15101–15113.
60 A. Barua, M. Samiur Rahman, A. Sannyal, M. Sharif Khan and S. Faraezi, *Comput. Theor. Chem.*, 2023, **1220**, 113979.
61 S. Faraezi, M. S. Khan, F. Z. Monira, A. Al Mamun, T. Akter, M. Al Mamun, M. M. Rabbani, J. Uddin and A. J. S. Ahammad, *ChemEngineering*, 2022, **6**, 27.
62 V. Subasinghege Don, L. Kim, R. David, J. A. Nauman and R. Kumar, *J. Phys. Chem. C*, 2023, **127**, 5920–5930.
63 *Synergy of adsorption and photosensitization of graphene oxide for improved removal of organic pollutants - RSC Advances*, RSC Publishing, DOI: **10.1039/C7RA01244F**, **https://pubs.rsc.org/en/content/articlehtml/2017/ra/c7ra01244f**, accessed 5 October 2025.